Molecular dynamics simulations of Li_xTiO_2 nanosphere as an anode electrode material

Blessing Rikhotso[1*] and *Phuti* Ngoepe[1]
[1]Materials Modelling Centre, University of Limpopo, Private Bag X 1106, Sovenga, 0727, South Africa

Abstract. This study uses molecular dynamics simulations to investigate the recrystallization and thermal stability of Li_xTiO_2 nanospheres ($Li_{0.11}TiO_2$, $Li_{0.15}TiO_2$, $Li_{0.19}TiO_2$, and $Li_{0.23}TiO_2$) as potential anode materials for lithium-ion batteries. Employing the Born-Mayer-Huggins interatomic potential, the simulations examined the structural evolution of the nanospheres during temperature cycling between 0 K and 2000 K, followed by controlled cooling. The results demonstrate that $Li_{0.11}TiO_2$, $Li_{0.15}TiO_2$, and $Li_{0.23}TiO_2$ form crystalline Ti-O layers upon recrystallization, while $Li_{0.19}TiO_2$ remains amorphous. During recrystallization, Li diffusion from the core to the surface, driven by Pauli repulsion, was observed in higher-lithium-content nanospheres. Analysis of cooled structures revealed that $Li_{0.11}TiO_2$, $Li_{0.15}TiO_2$ and $Li_{0.23}TiO_2$ maintained their structural integrity and exhibited both rutile and brookite channels. Radial distribution function analysis showed a consistent Ti-O bond length of approximately 2 Å across the temperature range. The findings suggest that Li_xTiO_2 nanospheres (excluding $Li_{0.19}TiO_2$) possess promising structural stability and crystallinity at varying temperatures and lithium concentrations, making them potential anode materials for lithium-ion batteries. The presence of both rutile and brookite phases, along with Li diffusion behavior, provides valuable insights for optimizing the design of high-performance Li_xTiO_2 anodes.

1 Introduction

Titanium dioxide (TiO_2) is an extensively acknowledged substance employed as a potentially advantageous anodic material for lithium-ion batteries, attributed to its abundant availability, economic viability, and environmentally benign characteristics [1][2][3]. Furthermore, TiO_2, exhibiting a substantial operational potential that surpasses 1.5 V, guarantees secure functionality by preventing lithium electroplating at lower potentials [4][5]. The structural robustness of TiO_2 remains remarkable throughout the lithium-ion intercalation and deintercalation processes [6]. Fundamentally, TiO_2 epitomizes a conventional lithium-ion intercalation compound, with its interaction with lithium represented in a simplified manner as:

* Corresponding author: nkateko.rikhotso@ul.ac.za

$$TiO_2 + x\,(Li^+ + e^-) \leftrightarrow Li_xTiO_2 \quad (0 \le x \le 1) \qquad 1$$

where x signifies the mole fraction of lithium ions within TiO_2. The maximum theoretical capacity of TiO_2 is quantified at 335 $mAhg^{-1}$ when x=1, which is attributed to the complete reduction of Ti^{4+} ions to Ti^{3+} ions [7]. Nevertheless, the insertion coefficient x generally approximates 0.5, correlating to a theoretical capacity of 167.5 $mAhg^{-1}$, due to the limited diffusion of lithium ions within orthorhombic $Li_{0.5}TiO_2$ [8]. The insufficient electronic conductivity along with the sluggish lithium-ion kinetics of bulk TiO_2 impedes their overall efficacy [9][10]. To augment the transport of lithium ions and electrons in TiO_2 anodes for commercial applications, a variety of nanosphere TiO_2 materials have been developed [11][12]. TiO_2 nanoarchitectures are meticulously engineered to yield titania nanomaterials with superior morphologies and nanoscale configurations, aimed at optimizing their properties [13]. The characteristics of nano-TiO_2 are influenced by their size, morphology, and crystalline polymorphism [14]. Existing research gaps remain concerning the enhancement of multiple facets of these nanomaterials for practical applications in energy storage and environmental remediation [15]. Li_xTiO_2 nanoarchitectures demonstrate enhanced lithium storage capabilities when juxtaposed with conventional graphite anodes, thus positioning them as a promising alternative for high-performance lithium-ion batteries [16].

The methodology of synthesis is critically significant in achieving the requisite properties associated with the crystallization and phase transformation of TiO_2. Crystallization is a fundamental aspect for the purification and manufacture of materials, with the crystalline structure being predominant in pharmaceutical products [17]. Regulating the crystallization process is essential to ensure uniform properties of the material. The dimensions and morphology of nanomaterials exert a profound influence on their optical, electronic, and catalytic characteristics [18].

The crystallization process, which encompasses nucleation and growth, plays a pivotal role in determining the structure, form, dimensions, and distribution of nanomaterials [19]. A more profound understanding of nanocrystal formation can facilitate improved management of various properties by manipulating crystallization conditions [8,20]. However, a significant discrepancy persists between theoretical models and experimental results, highlighting a major limitation inherent in nucleation theories [4,10]. $LixTiO_2$ nanoarchitectures exceed traditional graphite anodes in terms of lithium-ion uptake and transport, resulting in elevated capacities and rates [21]. The unique nanosphere of $LixTiO_2$ provides: Increased Surface Area: Enhances the contact area available for lithium-ion interaction. Reduced Diffusion Distances: Promotes expedited lithium-ion transport. Enhanced Structural Durability: Preserves structural integrity during the processes of lithium insertion and extraction [2,21].

These attributes significantly improve the overall capacity, operational efficiency, and cycling performance when contrasted with solid TiO_2. $LixTiO_2$ anodes exhibit elevated operating voltages (1.3-1.8 V relative to Li/Li^+), along with superior safety, cost-effectiveness, and environmental sustainability, thereby establishing them as a formidable alternative to graphite anodes [2]. The optimized nanosphere structure of $LixTiO_2$ plays an essential role in enhancing both ionic and electronic conductivities, which facilitates accelerated lithium-ion migration and improves charge transfer kinetics [2,21]. The complex micro-hierarchical architecture of $LixTiO_2$ ensures thermodynamic stability, a vital criterion for prolonged durability throughout cycling operations. The pseudocapacitive attributes of $LixTiO_2$ facilitate the accumulation of lithium ions on the anode surface, ultimately resulting in increased capacities and improved cycling stability.

2 Computational method

The recrystallization synthesis of Li_xTiO_2 nanospheres was simulated using molecular dynamics (MD) with the DL_POLY 4 program [2]. The Born-Mayer-Huggins (BMH) potential was chosen to describe interatomic interactions due to its ability to accurately model ionic materials.

$$U_{ij}(r) = \frac{q_i q_j}{r_{ij}} + A_{ij}\exp(-B_{ij}r) - \frac{C_{ij}}{r_{ij}^6} \qquad 2$$

The initial segment of the equation pertains to the Coulomb interaction, succeeded by the short-range repulsive forces between atomic nuclei, and ultimately, the van der Waals attraction is delineated. The ionic charges attributed to Lithium (Li), Titanium (Ti), and Oxygen (O) ions were quantified as +1, +4, and -2, correspondingly. The Ewald summation method was employed to ascertain the Coulomb potential, and the interatomic potential parameters were derived from the work of Rikhotso et al. [2] for all systems analyzed, with the Aij, Bij, and Cij values for the Li_xTiO_2 [20]. Table 1 summarises the composition, atomic number, Net Mass and Cell Volume of Li_xTiO_2.

The principal aim of this research was to thoroughly investigate the structural and microstructural characteristics of $LixTiO_2$ subsequent to recrystallization and the ensuing cooling processes. Each sample evaluated comprised more than 15,972 atoms. Amorphous TiO_2 nanospheres were selected due to their notable efficiency in capturing Li atoms, thereby facilitating the examination of structural attributes. Lithium ions were intercalated into TiO_2 nanospheres at varying concentrations (0.11 [600], 0.15 [800], 0.19 [1000], and 0.23 [1200] Li/Ti), as illustrated in Figure 1. The ion intercalation methodology developed by Kgatwane et al. [22] was pivotal in achieving a homogenous distribution of Li atoms through a systematic x, y, z trajectory, thereby mitigating Li accumulation. The impact of random Li intercalation on non-crystalline configurations can be observed in Figure 1b of the initial sample arrangements [22].

In order to enhance structural properties and energy storage capacities, recrystallization simulations were conducted at a temperature of 2000 K for $Li_{0.11}TiO_2$, $Li_{0.15}TiO_2$, $Li_{0.19}TiO_2$, and $Li_{0.23}TiO_2$ nanospheres. The simulation protocol encompassed: Temperature Cycling: Structures were subjected to a series of cooling and heating cycles ranging from 0 K to 2000 K in increments of 100 K. Computational Methods: NVT Ensemble: This approach was utilized to regulate the number of particles, the volume, and the temperature. Nosé-Hoover Thermostat: This apparatus was employed with a relaxation constant of 0.003 ps to ensure temperature stability. Verlet-Leapfrog Algorithm: This algorithm was applied with a time step of 1 fs to solve the equations of motion. Force Calculations: van der Waals Forces: These were computed with a proximity limit of 1 nm. Electrostatics: These were computed with a proximity limit of 2.1 nm [5]. Atomic positions and velocities were documented every 500 fs to facilitate comprehensive analysis. The radial distribution function (RDF) elucidates the probability density associated with the localization of an ion ii within a distance r from a designated particle j. The mathematical formulation for RDF can be articulated as follows:

$$g_{ij}(r) = \frac{V}{N_i N_j} \sum_j \frac{\langle n_{ij}(r - \Delta r/2,\, r + \Delta r/2)\rangle}{4\pi r^2 \Delta r}, \quad (3)$$

where V signifies the volume of the simulation cell, Ni and Nj represent the total quantities of ions i and j, respectively, and nij denotes the average quantity of ions j that encompass ion i at a distance $(r-\frac{\Delta r}{2}, r+\frac{\Delta r}{2})$ (4)

Table 1: The composition, atomic number, Net Mass (amu) and Cell Volume (Å^3)**.**

Sample Composition	Li	Ti	O	Total	Net Mass (amu)	Cell Volume (Å^3)
Pure TiO_2		Ti	O	15972	425377	1.04083 x 10^6
$Li_{0.11}TiO_2$	600	5324	10648	16572	424849	1.04083 x 10^6
$Li_{0.15}TiO_2$	800	5324	10648	16772	424673	1.04083 x 10^6
$Li_{0.19}TiO_2$	1000	5324	10648	16972	424497	1.04083 x10^6
$Li_{0.23}TiO_2$	1200	5324	10648	17172	424321	1.04083 x10^6

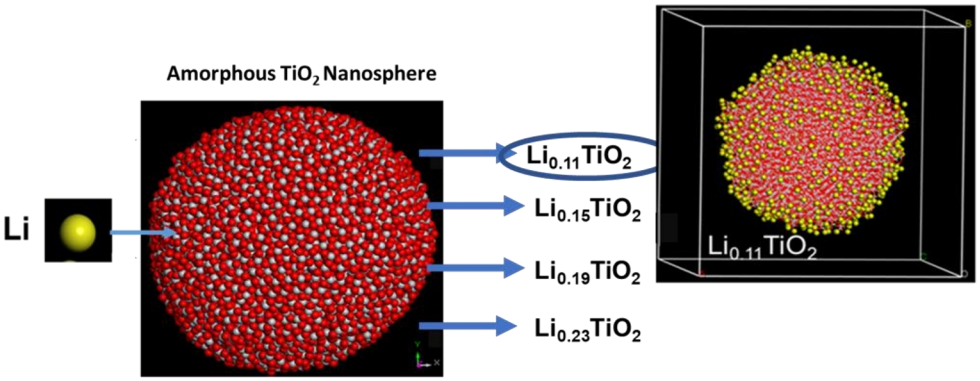

Fig. 1. An illustration depicting the interaction of Li atoms within amorphous TiO_2, forming Li_xTiO_2 nanospheres as initial structure samples.

2.1 Material analysis

The visualization of structural snapshots and microstructural layers pertaining to Li_xTiO_2 derived from molecular dynamics (MD) trajectories was executed utilizing Biovia Material Studio 2020. Through the application of Python scripts, the computations of X-ray diffraction (XRD) patterns were conducted, subsequently exhibited in Biovia Material Studio 2020, and analyzed in Sigma Plot. This analytical process was necessitated by the substantial presence of surface atoms on $LiTiO_2$ nanospheres during the recrystallization simulation synthesis procedure. Data extracted from DL_POLY output files, encompassing radial distribution functions (RDFs), diffusion coefficients, and activation energy barriers, were systematically compiled in Excel for comprehensive examination. Thereafter, Sigma Plot was utilized for the creation of all graphical representations [7].

3 Results and discussions

Molecular dynamics simulations of the recrystallization process revealed distinct structural outcomes depending on the lithium concentration in the Li_xTiO_2 nanospheres. Specifically, $Li_{0.11}TiO_2$, $Li_{0.15}TiO_2$, and $Li_{0.23}TiO_2$ formed crystalline Ti-O layers upon simulation at 2000 K, while $Li_{0.19}TiO_2$ remained amorphous (Figures 2 and 3). During recrystallization, outward diffusion of Li atoms from the core to the surface was observed, particularly pronounced in the higher-lithium-content $Li_{0.23}TiO_2$ nanospheres (Figure 2d). This Li expulsion is attributed to Pauli repulsion arising from shorter Li-Li bond distances at higher Li concentrations, exacerbated by electronegativity differences.

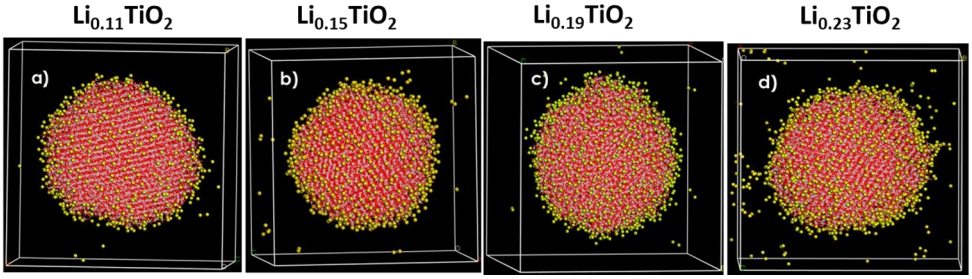

Fig. 2. Illustrates the recrystallized nanosphere architectures of $Li_{0.11}TiO_2$, $Li_{0.15}TiO_2$, $Li_{0.19}TiO_2$, and $Li_{0.23}TiO_2$.

Analysis of the recrystallized microstructures (Figure 3) confirmed crystal growth in $Li_{0.11}TiO_2$, $Li_{0.15}TiO_2$, and $Li_{0.23}TiO_2$. These structures exhibited a variety of lithium-ion distributions, including straight and zigzag tunnels, and both empty and Li-filled vacancies. Surface Li ions had a less significant impact on Ti-O coordination numbers compared to those within the microstructure. Vacancy formation in $Li_{0.11}TiO_2$, $Li_{0.15}TiO_2$, and $Li_{0.23}TiO_2$ was influenced by high enthalpy and entropy, leading to a reduction in Gibbs free energy and indicating an approach to equilibrium. In contrast, the disordered structure of $Li_{0.19}TiO_2$ nanospheres (Figure 2c and 3c) suggests a non-equilibrium state, potentially due to factors such as size, shape, electron distribution, or quantum-level pairing imbalances.

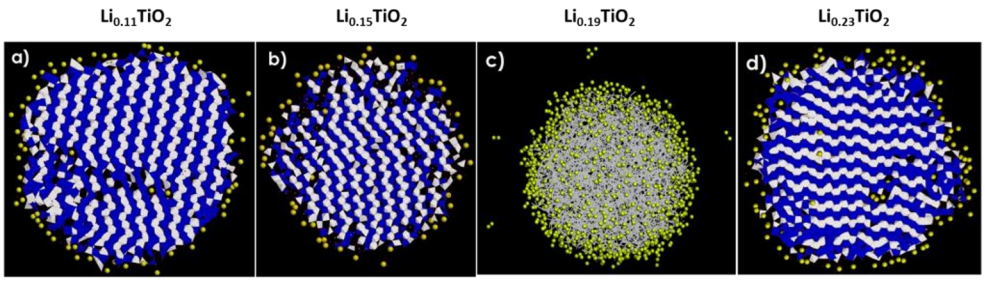

Fig. 3. Recrystallized microstructures of nanospheres for a) $Li_{0.11}TiO_2$, b) $Li_{0.15}TiO_2$, c) $Li_{0.19}TiO_2$, and d) $Li_{0.23}TiO_2$.

3.2.1. Li_xTiO_2 nanosphere

The Li_xTiO_2 nanospheres in figure 2 underwent structural cooling at temperatures of i) 1500 K, ii) 1000 K, iii) 500 K, and i) (0 K) indicated in figure 4 i), ii), iii) and iv) demonstrating a remarkable consistency in structural integrity across all investigated temperature variants. The microstructural analysis corroborated this homogeneity, emphasizing the exceptional

quality of the structural framework when juxtaposed with the recrystallization phase observed at 2000 K [1]. Notably, the microstructural snapshots in Figure 5 contain patterns of both linear (rutile) and zigzag (brookite) channels in figure 5 of 1 i) and ii), whereas only zigzag channels characteristic of brookite were detected in i) ii) and iv), thereby signifying the absence of the rutile phase at reduced temperatures [2]. Furthermore figure 5 of 1 and 3 for iii) and iv) revealed an increase in vacancies, encompassing both unoccupied and those occupied by Li ions, which were predominantly localized at the boundaries, in contrast to the observations seen in i) and ii).

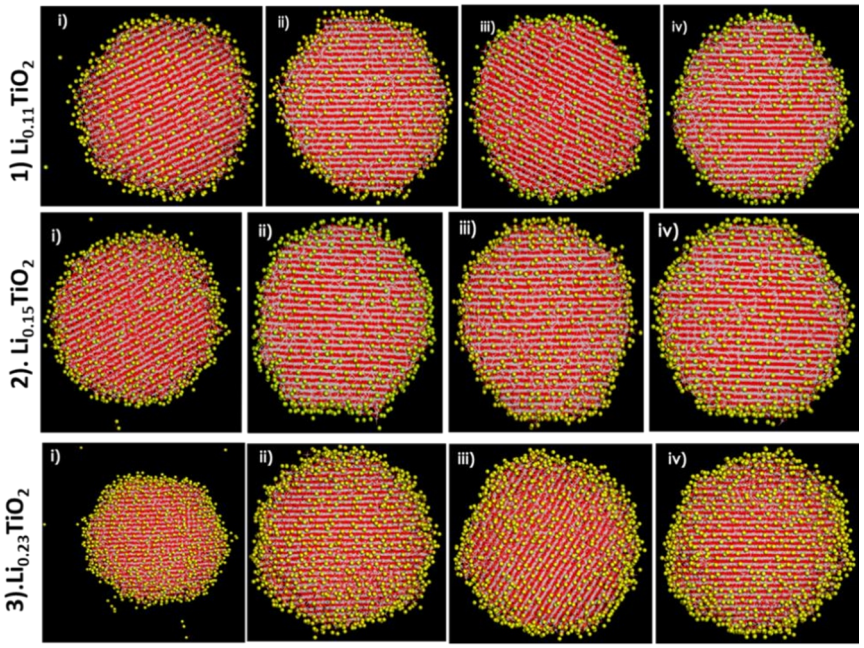

Fig. 4. Coooled 1. $Li_{0.11}TiO_2$, 2. $Li_{0.15}TiO_2$ and 3. $Li_{0.23}TiO_2$ nanospheres at i) 1500 K, ii) 1000 K, iii) 500 K, and iv) 0 K after being recrystallised.

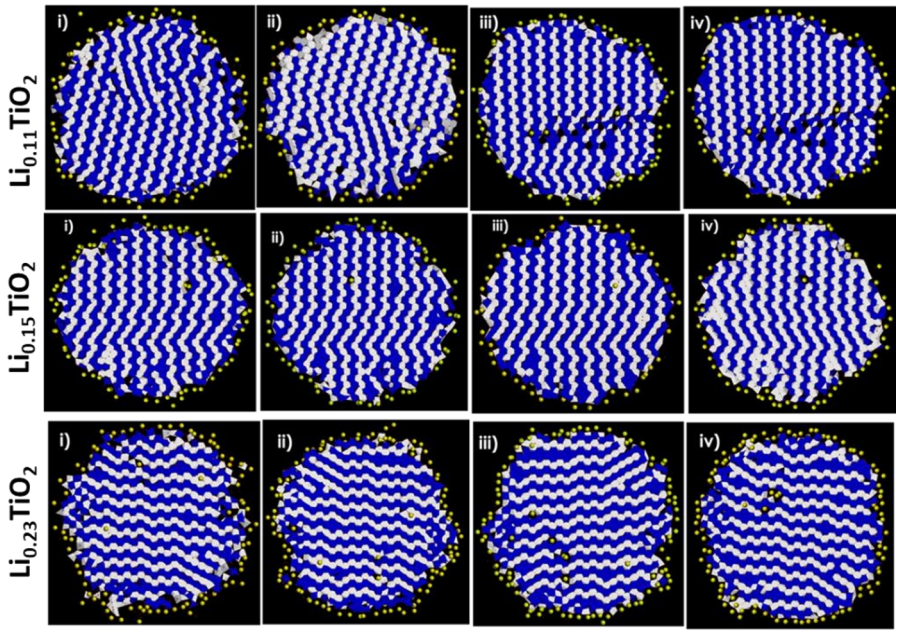

Fig. 5. Cooled $Li_{0.11}TiO_2$, $Li_{0.15}TiO$ and $Li_{0.23}TiO_2$ nanosphere microstructures at 1500 K, ii) 1000 K, iii) 500 K and iv) 0 K.

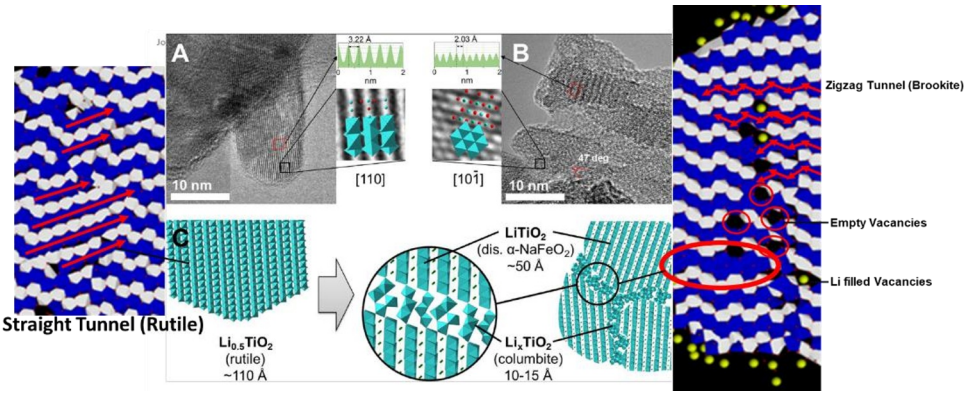

Fig. 6. Shows the TEM micrographs of nano-rutile chemically lithiated to (A) $Li_{0.5}TiO_2$ and (B) $LiTiO_2$ (C) schématique illustration of the structure and local disorder in Li rich nano-TiO_2 compared with the formation of nanosphere simulated microstructures Li_XTiO_2 [this work] at varying reduced temperatures, maintaining a consistent crystalline pattern [16].

The majority of lithium ions are located both within and on the exterior surfaces of the nanospheres across a range of temperature conditions, exhibiting minimal ionic migration [4]. The distinctly crystalline characteristics of the structures illustrated in Figures 4 i), ii), iii), and iv) are corroborated in Figure 7 i), ii), iii), and iv), which reveal the presence of characteristic linear and zigzag tunnels related to ructile and brookite polymorphs [5]. In Figures 5 of 1, 2, and 3, lithium ions are identified within tunnels and vacancies [6]. Regrettably, the cooled structures and microstructural features of $Li_{0.19}TiO_2$ nanospheres could not be presented due to unsuccessful recrystallization, as indicated in Figures 2 and 3 c) [7].

In order to investigate the structural behaviours, the $Li_{0.23}TiO_2$ nanosphere of figure 3. d) underwent a cooling process, as demonstrated in Figure 4 of 3 (i, ii, iii, iv) respectively . The accumulation of Li^+ ions on the surface, accompanied by restricted diffusion, can be observed in Figure 4 of 3 i) [8]. The structure undergoes contraction as a result of the elevated concentration of diffused lithium ions. Notably, even at reduced temperatures, Li^+ ions tend to persist on the surface and within the nanosphere, as emphasized in Figures 4 for 1), 2), and 3) [9]. The crystalline integrity of $Li_{0.23}TiO_2$ is largely preserved across all systems, particularly at 0 K, as illustrated in Figure 4 of 3 iv). A significant proportion of Li^+ ions are located both on the surface and within the structural matrix [10]. These observations are substantiated by microstructural cross-sections, which demonstrate structural integrity ranging from 1500 K to 0 K, as depicted in Figures 5 of 1, 2, and 3 i),ii),iii) and iv). The microstructure presented in Figure 5 of 3 i), ii), iii) and iv) and 6 reinforces the structural stability of $Li_{0.23}TiO_2$ throughout the cooling process, revealing linear and zigzag tunnels associated with rutile and brookite polymorphs, along with vacant Ti^{4+} sites, Li-occupied Ti^{4+} vacancies, and certain Li^+ ions positioned within the lower Ti^{4+} tunnels [11].

3.1.2. Li_xTiO_2 Nanosphere

Figure 7 presents visual depictions of the Radial Distribution Functions (RDFs) illustrating the interactions between Titanium (Ti) and Oxygen (O) pairs within nanospheres of Lithium-Titanium Oxide (Li-Ti-O) compounds, specifically $Li_{0.11}TiO_2$, $Li_{0.15}TiO_2$, $Li_{0.19}TiO_2$, and $Li_{0.23}TiO_2$, across a thermal spectrum ranging from absolute zero (0 K) to 2000 Kelvin (2000 K), all exhibiting a bond length approximating 2 Angstroms (Å). The investigation of the RDFs pertaining to the $Li_{0.11}TiO_2$ nanosphere, as illustrated in Figure 7. A), uncovers distinct peaks that demonstrate stability throughout the temperature continuum, with the most pronounced peak detected at 0 K and the least discernible peak identified at 2000 K, thereby indicating a trend of suitable crystalline structure formation [12]. A meticulous analysis of the amplified peaks situated within the 3 Å to 5 Å interval reveals that the structures of $Li_{0.11}TiO_2$, $Li_{0.15}TiO_2$, and $Li_{0.23}TiO_2$ manifest a significant degree of crystallinity at lower thermal states, with this crystalline characteristic progressively diminishing as the temperature rises [13]. Conversely, the $Li_{0.19}TiO_2$ nanosphere, as represented in Figure 7. C) exhibits features of non-crystallinity following the cooling procedure, with the extent of non-crystalline behavior intensifying as the temperature escalates [14]. The consistent preservation of structural crystallinity within the Titanium dioxide (TiO_2) nanospheres across diverse temperature conditions and Lithium ion (Li^+) concentrations, with the exception of the $Li_{0.19}TiO_2$ instance, suggests a promising potential for application as anode electrodes in Lithium-ion battery systems [15].

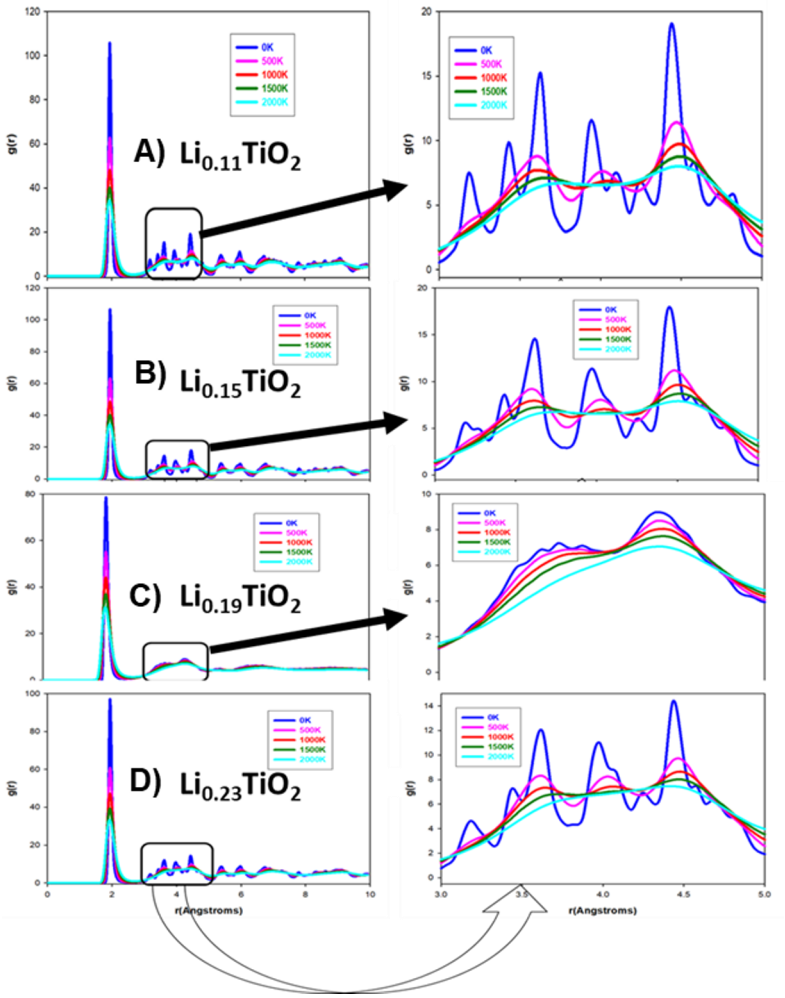

Fig. 7. Displays simulated RDF plots for the $Li_{0.11}TiO_2$ nanosphere at low and high temperatures, with an enlarged section between 3 and 5 Å for enhanced visualization.

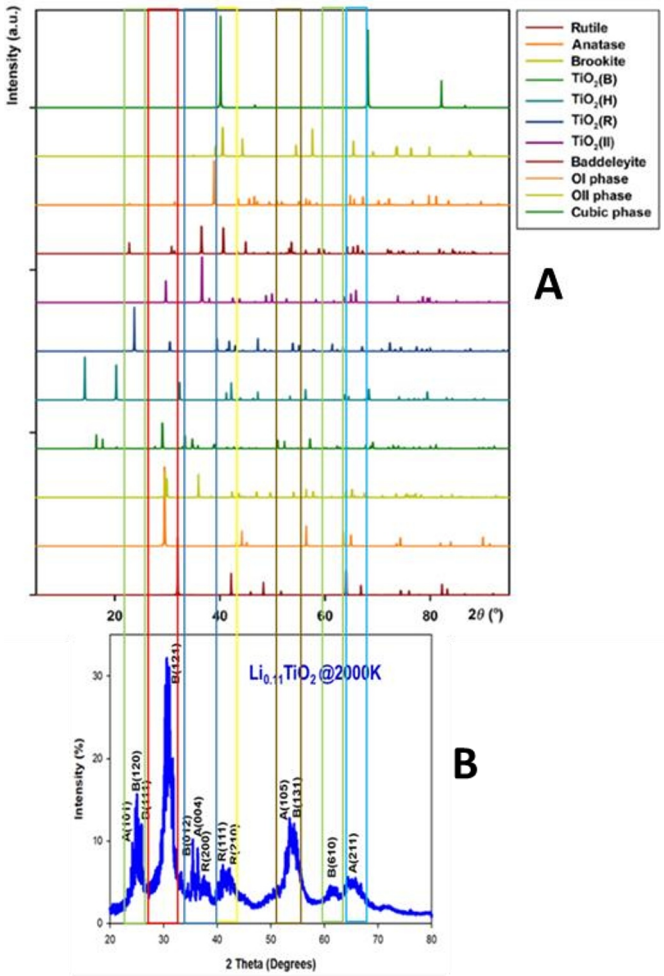

Fig. 8. Snapshots of A) experimental XRDs of pure TiO_2 materials superimposed with B) **s**imulated XRD patterns of $Li_{0.11}TiO_2$ and those in figure 9 for structural characterization [21].

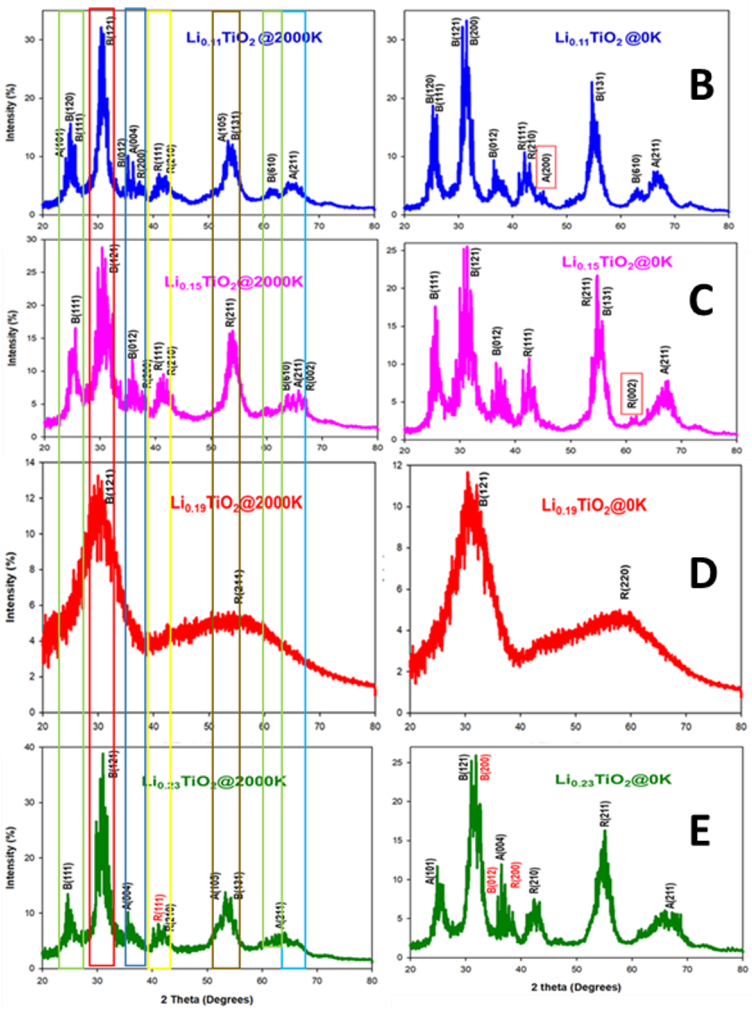

Fig. 9. Simulated XRD patterns of $Li_{0.11}TiO_2$, $Li_{0.15}TiO_2$, $Li_{0.19}TiO_2$, $Li_{0.23}TiO_2$ nanospheres at 2000 K and 0 K for structural characterization.

The X-ray diffraction (XRD) patterns acquired for the $Li_{0.15}TiO_2$ and $Li_{0.11}TiO_2$ nanospheres indexed to the pure TiO_2 are illustrated in Figures 8 and 9 B) and C), respectively, reveal analogous peak positions, albeit characterized by disparate frequencies and intensities. Within the $Li_{0.11}TiO_2$ nanosphere, the most significant peaks are discerned at 34% (2000 K) and 39% (0 K), while in the $Li_{0.15}TiO_2$ nanosphere, the peak maxima occur at 29% and 25% under the same thermal conditions. The predominance of brookite polymorphs is distinctly observable in the $Li_{0.15}TiO_2$ nanosphere across both thermal states, as depicted in Figure 9. c) [1]. However, the existence of multiple peaks at equivalent 2θ positions implies the coexistence of rutile and anatase phases, which pose challenges for differentiation due to closely spaced reflections and a limited set of indexable planes. The XRD patterns for both nanospheres corroborate the microstructural representations presented in Figures 5 of i) and iv) and 6 respectively [2]. In contrast to the XRD patterns of $Li_{0.11}TiO_2$, $Li_{0.15}TiO_2$, and $Li_{0.23}TiO_2$ nanospheres depicted in Figures 9 of B, C, and E, the XRD patterns for $Li_{0.19}TiO_2$ nanospheres showcased in Figure 9 D exhibit broad peaks, with principal indexed peaks occurring at 2θ values of 30° and 55°, correlating to the (121) and (211) (220) reflections of

brookite and rutile polymorphs, thereby indicating a pronounced amorphous characteristic at both 2000 K and 0 K, consistent with the XRD of pure TiO_2 and radial distribution function (RDF) of Ti-O pairs presented in Figure 6 and 7 respectively. The disordered configuration of Li, Ti, and O atoms allows for the observation of the microstructure of the recrystallized system alongside the structures at reduced temperatures, rendering the $Li_{0.19}TiO_2$ systems ill-suited for recrystallization and cooled synthesis due to their inadequate thermal stability [3]. The simulated XRD patterns for the $Li_{0.23}TiO_2$ nanosphere system at 2000 K and 0 K, as represented in Figure 9. E), disclosed intense peaks at 2θ values of 25°, 30°, 33°, 42°, 55°, 56°, and 65°, with a heightened intensity at 2000 K (39%) in comparison to 0 K (27%). These peaks correspond to reflections from the (111), (121), (200), (012), (004), (111), (210), (105), (131), and (211) planes of brookite, anatase, and rutile phases. The exclusive appearance of the (111) plane for rutile at 2000 K, alongside the (200)-(012) planes for brookite and the (200) plane for rutile at 0 K, indicates a phase transition from elevated to diminished temperatures [4]. The investigation of lithium transport within the nanosphere is pivotal for its efficacy as an anode material. This study examined the mobility of Li^+ ions across the temperature range of 0 K to 2000 K within the nanosphere (0-D) by computing diffusion coefficients at various thermal states and elucidating the activation energy requisite for Li^+ diffusion [5].

Figure 10 delineates the diffusion coefficients of lithium as a function of temperature within various compositions of $Li_{0.11}TiO_2$, $Li_{0.15}TiO_2$, $Li_{0.19}TiO_2$, and $Li_{0.23}TiO_2$ nanospheres. Throughout the temperature spectrum ranging from 100 to 1300 K, it was discerned that the $Li_{0.19}TiO_2$ nanospheres exhibited significantly elevated diffusion coefficients that remained non-zero when contrasted with the diffusion coefficients of the other specified samples. In contrast, the nanospheres corresponding to $Li_{0.11}TiO_2$, $Li_{0.15}TiO_2$, and $Li_{0.23}TiO_2$ revealed coefficients that were nearly indistinguishable from zero and demonstrated overlapping trends up to a temperature threshold of 700 K [6]. Importantly, upon attainment of temperatures surpassing 1200 K, it was observed that the diffusion coefficient for $Li_{0.23}TiO_2$ underwent an increase and subsequently began to deviate from the diffusion coefficients of both $Li_{0.11}TiO_2$ and $Li_{0.15}TiO_2$. Moreover, these two nanospheres, along with $Li_{0.19}TiO_2$, manifested characteristics suggestive of an amorphous phase and did not exhibit crystallization, as visually represented in Figures 2 and 3 c) [7].

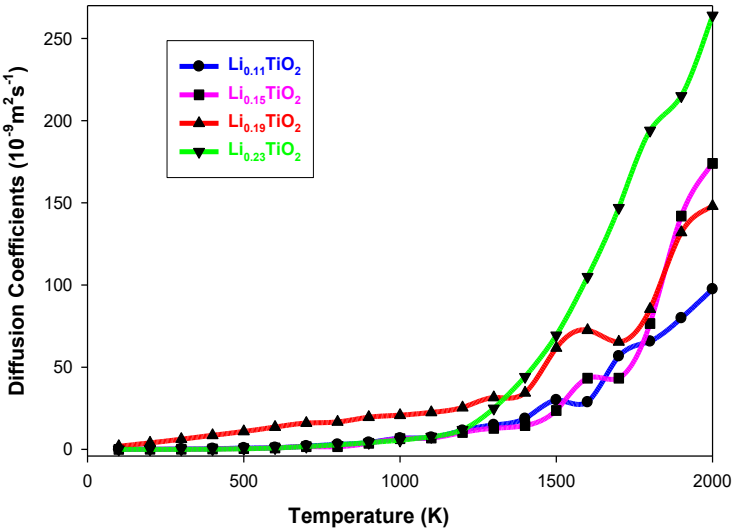

Fig. 10. Diagram of Li^+ diffusion coefficients at different temperatures in TiO_2 nanospheres with 0.11, 0.15, 0.19 and 0.23 Li^+ concentrations on the same axis.

The activation energies that have been computed for nanospheres of $Li_{0.11}TiO_2$, $Li_{0.15}TiO_2$, $Li_{0.19}TiO_2$, and $Li_{0.23}TiO_2$, spanning from 1.0 K^{-1} to 2.0 K^{-1}, exhibit values of 0.25 eV, 0.29 eV, 0.18 eV, and 0.37 eV, respectively, as depicted in Figure 11. Notably, the highest activation energy was determined for the $Li_{0.23}TiO_2$ nanosphere, with subsequent values decreasing for $Li_{0.15}TiO_2$ and $Li_{0.11}TiO_2$. Conversely, the lowest activation energy is associated with the $Li_{0.19}TiO_2$ nanosphere, indicating that it demands the least amount of energy for lithium activation within the specified temperature range of 1.0 K^{-1} to 2.0 K^{-1}. Consequently, this phenomenon has led to the attainment of elevated diffusion coefficients at reduced temperatures. This observation may be partially attributed to the presence of an amorphous phase in the $Li_{0.19}TiO_2$ nanosphere, preventing its recrystallization, as elucidated in Figures 2 and 3 c) [8].

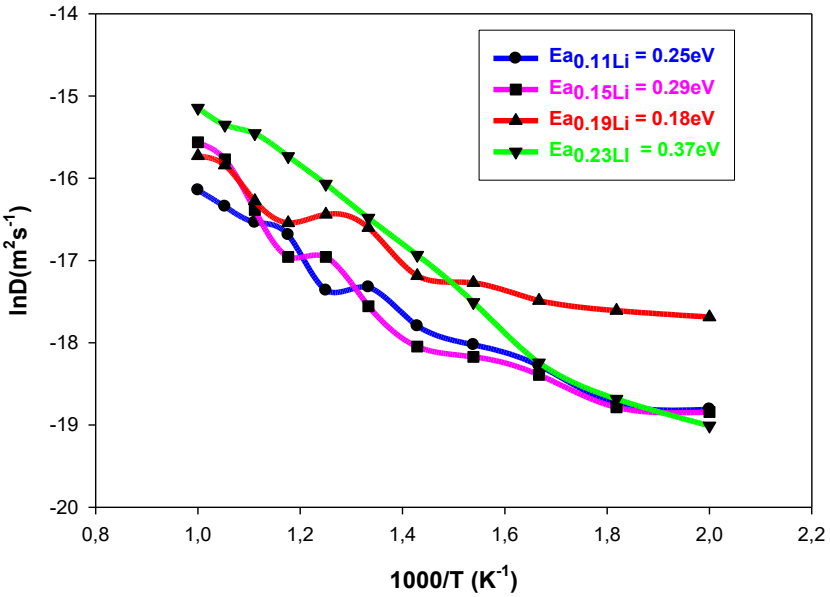

Fig. 11. Plots of lnD against 1000/T for Li_xTiO_2 nanospheres with x = 0.11, 0.15, 0.19, and 0.23.

4 Conclusions

Amorphous titanium dioxide (TiO_2) nanospheres, characterized as zero-dimensional (0D) structures, were integrated with varying lithium concentrations to engineer nanoarchitectures such as $Li_{0.11}TiO_2$, $Li_{0.15}TiO_2$, $Li_{0.19}TiO_2$, and $Li_{0.23}TiO_2$. These synthesized constructs underwent a recrystallization process at an elevated temperature of 2000 K, followed by a systematic cooling to absolute zero in intervals of 500 K, and were subsequently reheated to 2000 K in increments of 100 K. The majority of the lithium-doped TiO_2 samples, with the exception of $Li_{0.19}TiO_2$, demonstrated remarkable crystallization, as substantiated by Radial Distribution Functions (RDFs) and X-ray Diffraction (XRD) analyses, signifying a substantial degree of crystallinity even at reduced thermal conditions [1][2][3]. Microscopic investigations revealed the existence of both zigzag and linear tunnels within these structures, which correspond to the brookite and rutile polymorphs, respectively.

These tunnels acted as conduits for lithium-ion transport, a phenomenon that was further corroborated through XRD analyses performed at varying temperature regimes [4]. Within these tunnels, lithium ions occupied designated vacancies, thereby enhancing their mobility

within the structural matrix. Notably, the amorphous $Li_{0.19}TiO_2$ nanosphere did not demonstrate any indications of crystallization, as evidenced by RDF and XRD patterns that exhibited broad and pronounced peaks [5]. In terms of diffusion coefficients, it was discerned that for the majority of lithium concentrations and nanoarchitectures, the values remained near zero at lower temperatures, progressively increasing beyond 500 K, with a substantial escalation observed above 1000 K [6]. Conversely, the amorphous $Li_{0.19}TiO_2$ nanosphere manifested elevated diffusion levels at lower temperatures; however, this was eclipsed by the diffusion rates of other concentrations at higher temperatures [7]. The activation energies pertinent to lithium migration within the TiO_2 nanosphere structures corresponded closely with the established transport characteristics, thereby reinforcing their prospective application as anode materials in lithium-ion batteries, particularly during the charging and discharging cycles [8]

The authors acknowledge the Centre for High-Performance Computing (CHPC) in Cape Town under the National Integrated Cyberinfrastructure System (NICIS) and the Materials Modelling Centre (MMC) at the University of Limpopo for providing the computational resources essential for this work. The financial support from the Council for Scientific and Industrial Research (CSIR-MerSETA) is also acknowledged and greatly appreciated.

References

1. A. G. Dylla, G. Henkelman, A. J. Stevenson, Lithium Insertion in Nanostructured TiO2(B) Architectures, Acc. Chem. Res.,1**46,** 104 – 1112 (2013). https://pubs.acs.org/doi/10.1021/ar300176y
2. B.N. Rikhotso, M.G. Matshaba, D.C. Sayle, and P.E. Ngoepe, Simulated synthesis and structure of LixTiO2 nanosheets as anode material for lithium ion batteries, Opt. Mater.,**102**, 983 (2020). https://doi.org/10.1016/j.optmat.2020.109831
3. X. Wang, Y. Zhao, K. Mølhave and H. Sun, Engineering the Surface/Interface Structures of Titanium Dioxide Micro and Nano Architectures towards Environmental and Electrochemical Applications, Nanomaterials., **7**, 382 – 394 (2017). https://doi.org/10.3390/nano7110382
4. S. Paul, M.A. Rahman, S.B. Sharif, J.-H. Kim, S.-E.-T. Siddiqui, M.A.M. Hossain, TiO_2 as an Anode of High-Performance Lithium-Ion Batteries: A Comprehensive Review towards Practical Application, Nanomaterials.,**12**, 2034 (2022). http://dx.doi.org/10.3390/nano12122034
5. S. Wang, Y. Yang, Y. Dong, Z. Zhang and Z. Tang, Recent progress in Ti-based nanocomposite anodes for lithium ion batteriesJ. Adv. Ceram., 8, 1–18 (2019). https://doi.org/10.1007/s40145-018-0292-2
6. R. B. Godiksen, Z. T. Trautt, M. Upmanyu, J. Schiøtz and D. J. Jensen, S. Schmidt., Simulations of boundary migration during recrystallization using molecular dynamics., Acta Mater. **55** 6383–6391 (2007). https://doi.org/10.1016/j.actamat.2007.07.055
7. V. Arszelewska, Electrochemical stability of the next generation lithium batteries Arszelewska, (2021). https://repository.tudelft.nl/record/uuid:c1cfb42d-6472-499d-a41e-7c980058da2c
8. K. E. Aifantis, U. Ahuja and Y. W. Hong, Next-Generation Anodes for Secondary Li-ion Batteries. In: Aifantis, K.E. (Ed.), Wiley-VCH. (2022). https://doi.org/10.1002/9783527836703.ch6

9. R. Marchand, L. Brohan, and M. Tournoux, TiO_2(B) a new form of titanium dioxide and the potassium octatitanate $K_2Ti_8O_{17}$, Mater. Res. Bul., **15**, 1129–1133 (1980). https://doi.org/10.1016/0025-5408(80)90076-8
10. C. Lu, R. Fang, and Y. Gan, X. He, and Z. Xiao, H. Huang, and J. Zhang, and X. Xia, and W. Zhang, and Y. Xia., Facile Synthesis of Pre-Lithiated $LiTiO_2$ Nanoparticles for Quick Charge and Long Lifespan Anode in Lithium-Ion Batteries, ACS Appl. Mater. Interfaces,**16**, 898-906 (2024). https://doi.org/10.1021/acsami.3c16525
11. L. Zhang, H. Noguchi, D. Li, T. Muta, X. Wang, M. Yoshio, and I. Taniguchi, Synthesis and electrochemistry of cubic rocksalt Li–Ni–Ti–O compounds in the phase diagram of $LiNiO_2$–$LiTiO_2$–Li $[Li_{1/3}Ti_{2/3}]$ O_2, J. Power Sources.,**185** 534–541, (2008). https://doi.org/10.1016/j.jpowsour.2008.06.054
12. C. Wang, W. Zhang, M. Liu, L. Duan, B. Ma, X. Zhang, W. Li, Synthesis of $LiTiO_2$ Nanocrystals/Ordered Mesoporous Carbon Composite Hosts for High-Performance Lithium–Sulfur Batteries, Small Sci., (2023). https://doi.org/10.1002/smsc.202300093
13. K. Jiang, X. Hu, H. Sun, D. Wang, X. Jin, Y. Ren, and G. Z. Chen, Electrochemical Synthesis of $LiTiO_2$ and $LiTi_2O_4$ in Molten LiCl, Chem. Mater., **16**, 4324-4329 (2004). https://doi.org/10.1021/cm049610t
14. D. Shlimas, A. Kozlovskiy, and M. Zdorovets, Study of the formation effect of the cubic phase of $LiTiO_2$ on the structural, optical, and mechanical properties of $Li_{2\pm x}Ti_{1\pm x}O_3$ ceramics with different contents of the X component, J. Mater. Sci: Mater.Electron., **32**, 7410–7420 (2021). https://link.springer.com/article/10.1007/s10854-021-05454-z
15. H. D. Yang, Y.Y. Kang, P.P. Zhu, Q.W. Chen, Li. Yang, J.P. Zhou, Facile hydrothermal preparation, characterization and multifunction of rock salt-type $LiTiO_2$, J. Alloys Compd., **872**, 159759 (2021). https://doi.org/10.1016/j.jallcom.2021.159759
16. C. K. Christensen, M. A. H. Mamakhel, A. R. Balakrishna, B. B. Iversen, Y. M Chiang and D. B. Ravnsbæk., Order–disorder transition in nano-rutile TiO_2 anodes: a high capacity low-volume change Li-ion battery material., Nanoscale., **11**, 12347-12357 (2019). https://doi.org/10.1039/C9NR01228A
17. M.A. Gatou, A Syrrakou, N. Lagopati and E. A. Pavlatou., Photocatalytic TiO_2-Based Nanostructures as a Promising Material for Diverse Environmental Applications: A Review. Reactions., **5**, 135–194 (2024). http://dx.doi.org/10.3390/reactions5010007
18. J. Kang, X. Yang, Q. H., Z. Cai, L.M. Liu, and L Guo, Recent Progress of Amorphous Nanomaterials., Chem. Rev., **123**, 8859−8941 (2023). https://doi.org/10.1021/acs.chemrev.3c00229
19. X.Wang, L. Guo, SERS Activity of Semiconductors: Crystalline and Amorphous Nanomaterials. Angew. Chem., Int. Ed. **59**, 4231−4239 (2020). https://doi.org/10.1002/anie.201913375
20. Lu, K.; Wang, J. T. Crystallization Kinetics of Ni-P Glass Activation Energies for Nucleation and Growth of Nuclei. J. Mater. Sci., **23**, 3001−3005 (1988). https://link.springer.com/article/10.1007/BF00547482
21. H. Zhang, J.F. Banfield,Structural characteristics and mechanical and thermodynamic properties of nanocrystalline TiO_2, Chem. Rev., **114** 9613-9644 (2014). https://doi.org/10.1021/cr500072j
22. T. X. T. Sayle, K.M Kgatwane, P. E. Ngoepe and D. C. Sayle., 'Breathing-crystals' the origin of electrochemical activity of mesoporous Li–MnO_2, J. Mater. Chem. A., **4**, 6456–6464 (2016). https://pubs.rsc.org/en/content/articlelanding/2016/ta/c6ta01832g